


Article

Conceptual Models for Exploring Sea-Surface Temperature Variability Vis-à Long-Range Weather Forecasting

Sergei Soldatenko 

Arctic and Antarctic Research Institute, 199397 St. Petersburg, Russia; sergei.soldatenko@sympatico.ca

Abstract: This paper analyzes the ability of three conceptual stochastic models (one-box, two-box, and diffusion models) to reproduce essential features of sea surface temperature variability on intra-annual time scales. The variability of sea surface temperature, which is particularly influenced by feedback mechanisms in ocean surface–atmosphere coupling processes, is characterized by power spectral density, commonly used to analyze the response of dynamical systems to random forcing. The models are aimed at studying local effects of ocean–atmosphere interactions. Comparing observed and theoretical power spectra shows that in dynamically inactive ocean regions (e.g., north-eastern part of the Pacific Ocean), sea surface temperature variability can be described by linear stochastic models such as one-box and two-box models. In regions of the world ocean (e.g., north-western Pacific Ocean, subtropics of the North Atlantic, the Southern Ocean), in which the observed sea surface temperature spectra on the intra-annual time scales do not obey the ν^{-2} law (where ν is a regular frequency), the formation mechanisms of sea surface anomalies are mainly determined by ocean circulation rather than by local ocean–atmosphere interactions. The diffusion model can be used for simulating sea surface temperature anomalies in such areas of the global ocean. The models examined are not able to reproduce the variability of sea surface temperature over the entire frequency range for two primary reasons; first, because the object of study, the ocean surface mixed layer, changes during the year, and second, due to the difference in the physics of processes involved at different time scales.

Keywords: sea surface temperature; climate variability; ocean–atmosphere system; conceptual climate models; long-range weather forecasting



Citation: Soldatenko, S. Conceptual Models for Exploring Sea-Surface Temperature Variability Vis-à Long-Range Weather Forecasting. *J. Mar. Sci. Eng.* **2024**, *12*, 1483. <https://doi.org/10.3390/jmse12091483>

Academic Editors: João Miguel Dias and M^o Teresa de Castro Rodríguez

Received: 26 July 2024

Revised: 19 August 2024

Accepted: 23 August 2024

Published: 27 August 2024



Copyright: © 2024 by the author. Licensee MDPI, Basel, Switzerland. This article is an open access article distributed under the terms and conditions of the Creative Commons Attribution (CC BY) license (<https://creativecommons.org/licenses/by/4.0/>).

1. Introduction

Demand for information on climate predictions and weather forecasts with varying lead times has increased dramatically over the past few decades and is likely to grow even faster in the coming years. Driving this demand is the current climate change, which is occurring at an unprecedented rate and varies greatly across geographies. Consequently, normal (“typical”) weather conditions in different geographical regions are also changing rapidly, thereby directly and indirectly affecting people and all of their multifaceted and diverse activities [1]. For decades, numerical models of the atmosphere–ocean–land system of varying degrees of complexity have been used as the main tool for weather forecasting and climate prediction. However, we should realize that there is a fairly clear distinction between weather forecasting and climate prediction. In substance, the weather forecasting is a Cauchy or, in other words, initial-value problem, the solution to which is highly sensitive to the accuracy of imposing the initial conditions [2–6]. Here, the term “weather” refers to the daily conditions of the atmosphere as described by a number of atmospheric variables such as pressure, temperature, wind speed and direction, humidity, etc. It is important to note that due to the high sensitivity to initial conditions and the chaotic and multiscale nature of atmospheric dynamics, the weather forecast has a predictability limit [7–11]. Climate is an “average” weather in a particular region and, in a sense, is defined as an ensemble of states traversed by a climate system over a sufficiently long time

period [12], which is about 30 years, according to the World Meteorological Organization (WMO) [13]. The climate prediction, unlike the weather forecast, is a boundary-value problem, the solution to which depends mainly on the external forcing that forms the boundary conditions.

Beginning in the mid-20th century, atmospheric and oceanic explorations were largely stimulated by the development of computer technology, which was accompanied by the development of mathematical atmospheric and oceanic models and the emergence of a new direction in forecasting science—numerical weather prediction (NWP) for both short and medium ranges [14]. Since then, weather prediction has improved significantly due to the continuous enhancement of mathematical models of the atmosphere and the ocean, the exponential growth of computing power, as well as the growth in the volume of in situ and remote observations [15]. Despite advances in the study of the atmosphere and ocean and the availability of extremely complex high-resolution ocean–atmosphere models with increasingly accurate representations of physical processes, scientists have not been able to significantly increase the lead time for reliable weather forecasts, which is currently close to two weeks [16]). In general terms, predictability is the degree to which the state of the atmosphere can be accurately predicted. Although the reliability of numerical weather forecasting is limited to about two weeks, there is an urgent need for long-range and ultra-long-range forecasts to protect people, improve safety, and maintain the pace of socio-economic development.

In accordance with the classification adopted by the WMO, meteorological forecasts are divided into several categories [17]. The main goal of short-term weather forecasting is to predict the fields of meteorological variables, weather patterns, and hazardous weather phenomena such as heavy showers, tornadoes, fogs, local thunderstorms, etc. In the meantime, on longer time scales, the forecast objects are not the instantaneous values of meteorological variables associated with the word “weather”, but the probabilistic characteristics of the expected distributions, such as, for example, monthly and seasonally averaged anomalies of meteorological variables or the probabilities of anomaly gradations (below normal, normal, and above normal).

As the lead time of a weather forecast increases, it becomes critically important to correctly take into account interactions between the atmosphere and thermally inertial components of the Earth’s climate system, primarily the ocean. Understanding essential features of ocean dynamics is vital to long-range weather and climate prediction. Generally, the ocean, having high heat capacity, absorbs most of the solar radiation that reaches our planet and thereby represents a considerable heat storage reservoir. Since the solar radiation flux has a strong latitudinal dependence, the ocean receives the greatest amount of solar energy in the equatorial regions. Large-scale surface ocean currents, typically driven by the wind, transport the ocean’s accumulated heat throughout Earth, thereby controlling weather and climate conditions in various parts of the globe. The ocean conveyor belt is also a very important factor in the global distribution of heat energy, affecting and stabilizing climate on the entire planet. From the other perspective, changes in the Earth’s climate strongly alter the physical and chemical properties of the ocean. Suffice it to say that over the past 12 decades (from 1900 to 2019), the global mean sea surface temperature (SST) has increased by an average of 0.062 ± 0.013 °C per decade, while over the last decade (from 2010 to 2019), the SST warming rate speeded up to a value of 0.280 ± 0.068 °C, more than 4 times the long-range mean [18].

It should be emphasized that SST (T_w) is the most important physical quantity, which, on the one hand, describes the ocean state and dynamics, and, on the other hand, characterizes the features of the ocean’s impact on the atmosphere and the formation of long-term temporary changes in weather and climate. The SST field has significant spatial variability with a wide range of scales: global scale with amplitudes ΔT_w of tens and ones of degrees Celsius, including latitudinal variability and sharp contrasts in warm and cold surface currents; synoptic-scale with $\Delta T_w = 10^{-1} \dots 10^0$ °C (note that the ocean synoptic scale is a horizontal length l_H of the order of $10^1 \dots 10^2$ km); mesoscale ($l_H = 10^2 \dots 10^4$ m) with

$\Delta T_w \approx 10^{-1} \text{ }^\circ\text{C}$; and small-scale ($l_H \leq 10^1 \text{ m}$) with $\Delta T_w = 10^{-2}, \dots, 10^{-1} \text{ }^\circ\text{C}$. The SST field is also characterized by considerable temporal variability, namely inter-annual, which is mainly an integral of thermal effects of the atmosphere–ocean interaction; seasonal variability with periods of months, which is also an integral of the atmosphere–ocean interaction and can be formed due to the variability of the main ocean currents and upwelling; synoptic oceanic variability with periods of months and weeks generated by the oceanic synoptic eddies; synoptic atmospheric variability with periods of several days generated by storms, etc.; mesoscale variability with periods from hours to minutes generated by internal waves and clouds; and, finally, small-scale variability with periods from minutes to fractions of a second generated by surface waves and turbulence. The distribution of mean annual SST is, to a large degree, determined by the insolation that, in turn, strictly depends on the latitude. Since SST and its anomalies significantly affect long-term weather and climate conditions, it is very important to take into account both SST and its fluctuations in long-range weather forecasting and climate prediction (e.g., [19] and references therein).

The classical approach to NWP assumes the availability of mathematical models of the atmosphere, ocean, and active layer of land, built on a rigorous physical basis and described by systems of multidimensional partial differential equations. As we mentioned above, short- and medium-range weather forecasting is an initial value problem, which means that if the initial atmospheric state in a given geographical region or the entire planet is known, then by numerically integrating the NWP model equations, one can predict the future state of the atmosphere. Since the behavior of the atmosphere, due to its nonlinearity and extremely high sensitivity to initial conditions, is chaotic (the phenomenon of deterministic chaos [20]), the NWP time horizon is limited to approximately two weeks. Therefore, NWP models are commonly used for short-term and medium-range weather forecasting. In such problems, the ocean and active land layer are usually parameterized. For long-range weather forecasting, similar NWP (coupled atmosphere–ocean) models can be used. However, the skill of the long-term forecast obtained in such a way is quite low and difficult to understand and interpret. That is why long-range weather forecasts rely mainly on physically based statistical relations, and the forecast outputs are formulated in terms of probability that the climate variable will fall into above-normal, near-normal, or below-normal tercile. In addition, the wording of long-range weather forecasts is more general than short- or medium-range ones, since in this case the forecasts are not focused on all meteorological variables and phenomena, but mainly on time-space averaged values of temperature and precipitation. It should be emphasized that in recent years, AI technologies, primarily deep learning, which in essence is an artificial neural network with a number of layers, came to be seen by experts as promising tools for improving traditional forecasting models and developing completely new types of models for the purpose of weather and climate prediction (e.g., [21–24]).

In developing physical-statistical methods for long-range weather forecasting, a very important question arises: how to identify potential predictors for the analysis and forecast of a particular meteorological element or weather phenomenon in the region of interest? It is acknowledged (e.g., [25–28]) that SST and its anomalies strongly influence atmospheric circulation, thermal regime over continents, rainfall patterns, drought intensity and frequency, etc. In particular, tropical and subtropical Atlantic SST anomalies (SSTA) noticeably affect the weather and climate in the European middle and high latitudes, while Pacific SSTA influence weather patterns and climatic conditions in the North American region (e.g., [29–33] and references therein). The point is that SST significantly affects the heat and moisture content of the overlying air masses. Via large-scale atmospheric motions, heat, both sensible and latent, is transferred poleward from the tropics and subtropics to middle latitudes and then to polar regions, thereby influencing the regional weather and climate (e.g., [34,35] and references therein). This suggests that tropical and subtropical SSTA, along with some other variables, can be considered as predictors in developing statistical and AI-based long-range weather and climate prediction models for mid- and high latitudes.

The effects of tropical and subtropical SSTA and poleward heat transport on mid- and high-latitude weather and climate are mostly explored using coupled ocean–atmosphere models, including adjoint models (see Appendix A for details) perturbed by specified SST variations. However, this approach is computationally very expensive. Meanwhile, conceptual models of the climate system and its components (e.g., atmosphere and/or ocean) represent valuable tools for exploring the key physical processes and feedback that govern the climate system behavior, as well as for studying the cause-and-effect relationships between variables and forcings of various natures.

This paper aims to explore the influence of local effects due to ocean–atmosphere interactions on SST variability. In this study, SST variability is characterized by power spectral density, which is usually used to analyze the systems’ response to random perturbations. Conceptual stochastic models, which are valuable theoretical tools for exploring climate variability and predictability, were employed in the analysis.

2. Methods

Changes and variability in low-latitude SST, as earlier mentioned, is an important factor that to a certain extent influences large-scale atmosphere–ocean interaction, affecting weather patterns in extratropics and even in polar areas. Meanwhile, numerous studies show that SST variability is significantly affected by atmospheric circulation (e.g., [36–41]). For example, in the mid-latitudes, on seasonal to interannual time scales, the formation of large-scale SSTA is due to the variability of sensible and latent heat fluxes on the ocean surface, which, in turn, are closely related to the large-scale atmospheric dynamics. To explore SST and its variability, we can use the heat budget equation for the ocean surface mixed layer (ML), describing essential physical processes that drive the SST changes. Under the Boussinesq and incompressibility approximations, we can write the heat budget equation for ML as follows (see [42,43] for details):

$$h \frac{\partial T_{avg}}{\partial t} + h \mathbf{V}_{avg} \cdot \nabla T_{avg} + \nabla \cdot \int_{-h}^0 \hat{\mathbf{V}} \hat{T} dz + (T_{avg} - T_{-h}) \left(\frac{\partial h}{\partial t} + \mathbf{V}_{-h} \cdot \nabla h + w_{-h} \right) = \frac{Q_{net}}{\rho_w c_p^w} \quad (1)$$

Here h is the ML depth; T is the seawater temperature; ρ_w and c_p^w are the density and specific heat capacity of seawater, respectively; w is the vertical velocity; \hat{T} is the deviation from the vertically averaged temperature; $\hat{\mathbf{V}}$ is the deviation from the vertically averaged horizontal velocity \mathbf{V}_{avg} ; Q_{net} is the net heat flux across the ocean surface. Subscript avg denotes a vertically averaged quantity, while subscript $-h$ denotes the quantity at the ML lower boundary, therefore w_{-h} is the (large scale) entrainment velocity.

To advance our understanding of weather formation processes on long-range time scales, local SSTA need to be further explored since they can trigger responses in distant regions. Moreover, these responses can even be global if the SSTA are quite large. It is clear that in the upper ocean layer, which includes the ML and thermocline, vertical temperature changes are much greater than the horizontal ones. Consequently, changes in local thermodynamic conditions are driven much more by local energy/momentum exchange between the atmosphere and ocean, and vertical mixing rather than by horizontal transport and mixing. For this reason, to describe local SST variations, Equation (5) can be used in a somewhat simplified form.

Firstly, it can be assumed that vertical turbulent mixing “very quickly” levels out the temperature profile in the ML, so that if we consider processes with a characteristic time of one day or more, then the ML can be considered vertically well mixed with almost uniform salinity and temperature. Secondly, we can suppose that the ML is a horizontally homogeneous layer; therefore, the horizontal transport and diffusion can be neglected. Thirdly, we can also assume that SST variations are mainly determined by heat and momentum fluxes at the ocean–atmosphere interface, while the entrainment effects and changes in ML depth play a secondary role in the formation of local SST fluctuations; consequently, with sufficiently high accuracy, these processes can also be neglected. In view of the above, the local heat budget Equation (1) can be rewritten as [44–47]:

$$\frac{\partial T_w}{\partial t} + \frac{1}{h}(T_w - T_{-h})w_{-h} = \frac{Q_S - Q_{-h}}{\rho_w c_p^w h}, \tag{2}$$

where T_w denotes the SST; Q_S is heat flux through the ocean surface, which is given by:

$$Q_S = I_o(1 - \alpha) / 4 + (F_A - F_S) - H_S - LE_S. \tag{3}$$

Here $I_o(1 - \alpha) / 4$ is the incoming shortwave radiation at the ocean surface, where I_o is the solar constant and α is the planetary albedo; the difference $(F_A - F_S)$ is the net longwave radiation, where F_S the upward longwave radiation emitted by the ocean surface to the atmosphere and F_A is the atmospheric longwave counter-radiation; H_S is the upward surface turbulent sensible heat flux; LE_S is the upward surface turbulent latent heat flux due to evaporation at rate E_S , where L is the specific latent heat of evaporation. In (2), Q_{-h} is the turbulent entrainment heat flux through the bottom of ML and is defined as by $Q_{-h} = \rho_w c_p^w w_b (T_w - T_{-h})$, where w_b is the entrainment velocity [46]. Let us note that Equation (3) will be used to describe SST variability at temporal intervals significantly exceeding the characteristic time of atmospheric synoptic phenomena.

Sensible heat exchange between the ocean surface and atmosphere can be estimated by using the bulk aerodynamic formula (e.g., [48]):

$$H_S = -c_p^a \rho_a C_H |\mathbf{u}| (T_a - T_w) = -\vartheta_H (T_a - T_w), \tag{4}$$

where T_a is the near-surface air temperature; ρ_a is the air density; c_p^a is the air specific heat capacity at constant pressure; \mathbf{u} is the near-surface wind vector; and C_H is the bulk transfer coefficient for sensible heat.

The latent heat flux can be parameterized in a similar way

$$LE_S = -\rho_a LC_E |\mathbf{u}| [q_a - q_m(T_w)] = -\rho_a LC_E |\mathbf{u}| [r_q q_m(T_a) - q_m(T_w)], \tag{5}$$

where q_a is the air specific humidity; q_m is the saturation specific humidity at a given temperature; r_q is the air relative humidity; and C_E is the bulk transfer coefficient for moisture.

Let us assume that the relative humidity of the surface layer is close to 100%. Then, bearing in mind the small deviations of ocean water temperature from the air temperature, and using the Magnus formula, we can obtain $LE_S \approx -\vartheta_E (T_a - T_w)$. The long-wave heat budget component can be calculated using semi-empirical formulas $F_A - F_S = \gamma_q \gamma_n \sigma T_a^4 - \sigma T_w^4$, where σ is the Stefan–Boltzmann constant, γ_q and γ_n are coefficients accounting for the effects of water vapor and cloudiness on atmospheric counter-radiation. Expanding σT_a^4 in a Taylor series about T_w and retaining only the linear term, we approximately obtain $F_A - F_S \approx \vartheta_F (T_a - T_w)$. As a result, the heat balance Equation (2) can be represented as follows:

$$C_0 \frac{dT_w}{dt} = -\lambda T_w + \varepsilon. \tag{6}$$

where $C_0 = c_p^w \rho_w h$ is the effective heat capacity of the ocean ML; λ is the parameter characterizing feedback in the atmosphere–ocean system that also includes the effects of oceanic processes; ε is a parameter representing the residual terms. Expressions for these parameters are given below.

Let us decompose SST and other meteorological variables into seasonal and synoptic (order of days) parts, and also divide heat fluxes at the ocean surface into slow (seasonal) and short-periodic (synoptic) components. Then, applying the time averaging procedure to Equation (6), subtracting the resulting averaged equation from (2) and neglecting fluctuations in the feedback parameter λ , we can obtain the equation for SSTA T'_w [46,49–51]:

$$C_0 \frac{dT'_w}{dt} = -\lambda T'_w + \varepsilon', \tag{7}$$

where

$$\lambda = \vartheta_H + \vartheta_E + \vartheta_F + \rho_w c_p^w w_{-h}, \tag{8}$$

$$\varepsilon' = Q_0 Q' (1 - \alpha) + (\vartheta_H + \vartheta_E + \vartheta_F) T_0 T'_a - Q_{-h,0} Q'_{-h}. \tag{9}$$

Here, dimensionless coefficients of variation in solar radiation flux Q' , air temperature T'_a and heat exchange intensity due to the entrainment process Q'_{-h} are introduced, multiplied by the corresponding scale factors, indicated by the subscript "0". Recall that the coefficient of variation c' is the ratio of the standard deviation σ to the mean μ , $c' = \sigma/\mu$.

In order to estimate the parameters of Equations (7)–(9), we shall assume that $c_p^a = 10^3 \text{ Jkg}^{-1}\text{K}^{-1}$, $\rho_a = 1 \text{ kgm}^{-3}$, $C_H = 10^{-3}$, $|\mathbf{u}| = 5 \text{ ms}^{-1}$ [52], $h_0 = 70 \text{ m}$; $c_p^w = 4.2 \times 10^3 \text{ Jkg}^{-1}\text{K}^{-1}$ and $\rho_w = 10^3 \text{ kgm}^{-3}$. Then we have $C_0 \approx 2.9 \cdot 10^8 \text{ Jm}^{-2}\text{K}^{-1}$ and $\vartheta_H \approx 5 \text{ Wm}^{-2}\text{K}^{-1}$. To estimate the parameter ϑ_E , we use the Bowen ratio $\beta = H_S/LE_S$. Since over the tropical oceans the Bowen ratio is typically 0,1, while over the mid-latitude oceans it is slightly bigger, we shall assume that the annual $\beta \approx 0.2$ [53] then $\vartheta_E = \vartheta_H/\beta \approx 25 \text{ Wm}^{-2}\text{K}^{-1}$. The value of ϑ_F is taken to be $\vartheta_F \approx 5 \text{ Wm}^{-2}\text{K}^{-1}$ [46]. As an estimate of the entrainment velocity, we can take the value of 10^{-7} ms^{-1} [54]. It should be noted that the effect of entrainment at the lower boundary of ML depends on the intensity of turbulence in it, which is determined by the wind speed in the surface layer of the atmosphere. Consequently, the entrainment effect has a clear diurnal cycle, and its day-to-day variability is determined by meteorological synoptic variations with a characteristic time in the order of several days. In such a case, the entrainment effect can be neglected with sufficient accuracy. Since the parameters ϑ_H , ϑ_E and ϑ_F are subject to a high degree of uncertainty, their values obtained above can only be used for qualitative estimates of SST variability but not for accurate modeling and forecasting. By the way, if we assume that $T_a - T_w = 1 \text{ }^\circ\text{C}$ [55], then the resulting sensible and latent heat fluxes are in good agreement with the available observational data [56].

The ratio λ/C_0 , which is the reciprocal of the relaxation time τ_T , has the dimension of frequency and characterizes the aggregated effect of feedback in the atmosphere–ocean system and its thermal inertia. Using the given parameter values, we find that $\lambda/C_0 \approx 1.2 \cdot 10^{-7} \text{ s}^{-1}$, and, therefore, the relaxation time is $\tau_T \approx 3 \text{ mo}$. The variability of SSTA described by Equation (7) is driven by various physical processes covering a fairly wide range of time scales. In this paper, we shall consider the case when the correlation time τ_ε of the process $\varepsilon'(t)$ is much less than the characteristic time of the process $T'_w(t)$, i.e., $\tau_\varepsilon \ll \tau_T$. For this reason, Equation (7) can be interpreted as a stochastic Langevin equation that is used in atmospheric, oceanic, and climate research (e.g., [49,57–62]). Random process $\varepsilon'(t)$ can be treated as a delta-correlated (in time) random process, for which the correlation function is given by $R_\varepsilon(\tau) = \langle \varepsilon(t)\varepsilon(t') \rangle = 2D_\varepsilon\delta(t - t')$. Here, $\delta(\cdot)$ is the Dirac delta function, and D_ε is the diffusion coefficient, defined as $D_\varepsilon = \int_0^\infty R_\varepsilon(\tau)d\tau = \sigma_\varepsilon^2\tau_\varepsilon$, where σ_ε^2 is the variance of a delta-correlated random process [63].

To account for the effect of deep ocean layers on SST variations, multilayer ocean models can be used. The simplest one is the two-box model, the equations of which can be represented as follows [64,65]:

$$C_0 \frac{dT'_w}{dt} = -\lambda T'_w - \gamma(T'_w - T'_D) + \varepsilon', \tag{10}$$

$$C_D \frac{dT'_D}{dt} = \gamma(T'_w - T'_D), \tag{11}$$

where T'_D is the deep ocean temperature anomaly; $\gamma = 0.73 \text{ Wm}^{-2}\text{K}^{-1}$ is the coupling strength parameter; and $C_D \approx 3.3 \cdot 10^9 \text{ Jm}^{-2}\text{K}^{-1}$ is the effective heat capacity of the deep ocean layer [66].

The heat diffusion model applied to a semi-infinite medium is also a convenient theoretical tool for studying the influence of deep oceans on SST variability [67]:

$$\frac{\partial T'}{\partial t} = \alpha \frac{\partial^2 T'}{\partial z^2}, \quad \kappa \frac{\partial T'}{\partial z} \Big|_{z=0} = -\lambda T' + \varepsilon', \tag{12}$$

where $\alpha = 1.0 \times 10^{-4} \text{ m}^2\text{s}^{-1}$ is the thermal conductivity; $\kappa = \alpha c_p^w \rho_w$ is the heat diffusivity of the ocean. Recall that in the notations used in this paper $T'|_{z=0} = T'_w$ [54,68].

As is known, simple models such as those discussed above are very convenient and valuable tools for exploring fundamental climate-forming processes, contributing to a better understanding of the role of various physical mechanisms in the formation of weather and climate. The latter is very important from the point of view of developing methods for long-term weather and climate forecasts.

3. Results and Discussion

Equation (7) describes the seasonal dynamics of SSTA (“slow” process) affected by short-periodic (“fast”) synoptic processes represented by random forcing ε' . In fact, seasonal changes in SST are driven by a variety of physical processes spanning a wide range of timescales, from seconds to weeks. Examples of such processes are microscale turbulence, mesoscale processes (atmospheric fronts, cloud convection clusters), and synoptic scale phenomena (atmospheric waves and eddies with a time scale of several days and a spatial scale of several hundred kilometers). The deterministic effect of daily variations in meteorological variables also makes a tangible contribution to changes in SST. Longer-term events of various origins can also make a certain contribution to seasonal SST variations, such as the Madden–Julian oscillations in the tropics, fluctuations in monsoon intensity, the index cycle (in mid-latitudes), the periods of which vary from three to eight weeks, etc.

Stochastic Equation (7) determines the realization of random process $T'_w(t)$, which, due to its randomness, is uninformative. For this reason, we are more interested not in the realization of a random process itself but in its probabilistic characteristics. A suitable instrument for modeling and statistical study of random processes is the power spectral density function (PSD), which represents the signal power (variance) as a function of frequency [69,70]. PSD can be determined from the transfer function of the system in question, when the input is an applied random signal: $S_T^{(1)}(\omega) = |H^{(1)}(\omega)|^2 S_\varepsilon$ [71], where $S_T^{(1)}(\omega)$ is the PSD of SST fluctuations; $H^{(1)}(\omega)$ is the transfer function of system described by Equation (7); ω is the real angular frequency; S_ε is the PSD of random process $\varepsilon'(t)$, which can be obtained through the Wiener–Khinchin theorem [70]:

$$S_\varepsilon = \frac{1}{2\pi} \int_{-\infty}^{\infty} e^{-i\omega\tau} R_\varepsilon(\tau) d\tau = \frac{\sigma_\varepsilon^2 \tau_\varepsilon}{\pi}. \tag{13}$$

The Fourier transform of both sides of Equation (7) yields the transfer function from forcing ε' to SSTA T'_w :

$$H^{(1)}(\omega) = \frac{1}{i\omega C_0 + \lambda}. \tag{14}$$

Then the SST power spectrum is

$$S_T^{(1)}(\omega) = \frac{1}{\pi} \frac{q_\varepsilon^2 / C_0^2}{\omega^2 + (\lambda / C_0)^2}, \tag{15}$$

where $q_\varepsilon^2 = \sigma_\varepsilon^2 \tau_\varepsilon$.

Power spectrum (15), driven by random forcing ε' , is well known to climatologists, meteorologists, and oceanographers: at high frequencies ($\omega \gg \lambda / C_0$), PSD is proportional to ω^{-2} (“red noise”) and does not depend on feedbacks and ocean thermal inertia, while at low frequencies ($\omega \ll \lambda / C_0$) the spectrum is nearly constant. Thus, the ratio λ / C_0

determines the angular frequency $\omega_c = \lambda/C_0$ at which the transition from one mode to another occurs. The corresponding period of SST oscillations is $t_c \approx 3$ mo.

Since, as mentioned above, forcing is generated by short-periodic synoptic-scale oscillations, we can assume that $\tau_\varepsilon = 5$ days, i.e., over relatively long time intervals, the coherence within the series of meteorological and climatic observations vanishes and forcing simply becomes a stationary delta-correlated process [72]. Determining the variance of random forcing σ_ε^2 , generally speaking, is a non-trivial problem. In our study, forcing represents the cumulative effect of several uncorrelated random processes, such as short-term fluctuations in solar radiation fluxes, air temperature fluctuations, which largely determine changes in sensible and latent heat fluxes, fluctuations in surface wind velocity, which indirectly affect water entrainment from the thermocline, etc. Each of these random processes is characterized by a certain variance σ_i^2 . Consequently, the variance of cumulative forcing is equal to $\sigma_\varepsilon^2 = \sum_{(i)} \sigma_i^2$. The variances σ_i^2 can be derived from observations of variations in solar radiation fluxes, surface air temperature, the intensity of heat exchange between the ML and the thermocline, etc. It is quite clear that the resulting estimates can vary greatly across seasons and geographical regions. Therefore, for the sake of simplicity, we make use of the estimate $\sigma_\varepsilon \approx 1.5 \times 10^2 \text{Wm}^{-2}$ [46,73].

At relatively long time intervals $t \gg \tau_\varepsilon$, SST changes acquire the character of steady-state irregular fluctuations, and the process described by Equation (7) becomes stationary, whereby the SST variance does not depend on time and can be obtained by integrating the PSD of SST fluctuation $S_T^{(1)}(\omega)$ over the entire frequency domain [70]:

$$\sigma_T^2 = \int_{-\infty}^{\infty} S_T^{(1)} d\omega = \frac{\sigma_\varepsilon^2 \tau_\varepsilon}{\lambda C_0}. \tag{16}$$

By substituting the values of all parameters into the above formula, we can find the standard deviation of steady-state SST fluctuations: $\sigma_T = 0.98$ °C. This value looks quite realistic and corresponds to observational data. It is clear that this value can be more reliably estimated for a specific season and region. To estimate the effect of uncertainty in the parameter λ on σ_T , we logarithmically differentiate both sides of Equation (16) with respect to λ , and obtain

$$\frac{1}{\sigma_T} \frac{\partial \sigma_T}{\partial \lambda} \approx -\frac{1}{2\lambda}. \tag{17}$$

Thus, a minor variation $\Delta\lambda$ in the parameter λ results in a small fractional change $\Delta\sigma_T/\sigma_T$ in the standard deviation of SST, namely $\Delta\sigma_T/\sigma_T \approx -\Delta\lambda/2\lambda$. Taking the value of λ found above as a reference value, we find that a change in the parameter λ by $1 \text{Wm}^{-2}\text{K}^{-1}$ (which is about 3% of the reference value of λ) leads to a change in σ_T by 1.4%.

To estimate the effect of uncertainty in the parameter λ on SST power spectrum, we use the sensitivity function defined as a partial derivative of $S_T^{(1)}$ with respect to λ :

$$\Psi_\lambda^{(1)}(\omega) = -\frac{2q_\varepsilon^2}{\pi} \frac{\lambda}{(\lambda^2 + \omega^2 C_0^2)^2}. \tag{18}$$

The transfer function of the two-box model can be found by taking the Fourier transform of Equations (10) and (11):

$$H^{(2)}(\omega) = \frac{i\omega C_D + \gamma}{C_0 C_D [2i\omega\beta + (\omega_0^2 - \omega^2)]}. \tag{19}$$

where $\omega_0 = \sqrt{\gamma\lambda/C_0C_D}$ is the natural frequency and $\beta = [\lambda C_D + \gamma(C_0 + C_D)]/C_0C_D$ is the damping coefficient of the overdamped harmonic oscillator described by Equations (10) and (11). The corresponding power spectral density is of the form:

$$S_T^{(2)}(\omega) = \frac{1}{\pi} \frac{q_\varepsilon^2 (\omega^2 C_D^2 + \gamma^2)}{4\omega^2 \beta^2 + (\omega_0^2 - \omega^2)^2}. \tag{20}$$

By differentiating this equation with respect to λ , we obtain a sensitivity function that allows us to estimate the influence of variations in the parameter λ on the SST power spectrum:

$$\Psi_\lambda^{(2)}(\omega) = -\frac{2q_\varepsilon^2}{\pi C_0^2 C_D^2} \frac{\gamma^2 + C_D^2 \omega^2}{[(\omega_0^2 - \omega^2)^2 + 4\beta^2 \omega^2]^2} \frac{2\lambda\beta\omega^2 + (\omega_0^2 - \omega^2)\omega_0^2}{\lambda C_0}. \tag{21}$$

For the two-box model, the SST variance is derived by integrating $S_T^{(2)}(\omega)$ over frequency from negative infinity to positive infinity:

$$\sigma_T^2 = \int_{-\infty}^{\infty} S_T^{(2)} d\omega = \frac{\sigma_\varepsilon^2 \tau_\varepsilon}{\lambda C_0} \frac{\gamma C_0 + \lambda C_D}{(\gamma + \lambda) C_D + \gamma C_0}. \tag{22}$$

Next, consider heat diffusion model (12). The transfer function from stochastic forcing ε' to SSTA $T'(t, z)|_{z=0}$ is of the form:

$$H^{(3)}(\omega) = \frac{1}{\lambda + \sqrt{i} (\kappa \rho_w c_p^w \omega)^{1/2}}. \tag{23}$$

The expression for the power spectral density is, respectively

$$S_T^{(3)}(\omega) = \frac{1}{\pi} \frac{q_\varepsilon^2}{\lambda^2 + \lambda \sqrt{2\kappa \rho_w c_p^w \omega} + \kappa \rho_w c_p^w \omega}. \tag{24}$$

Power spectrum sensitivity can be estimated by the following sensitivity function:

$$\Psi_\lambda^{(3)}(\omega) = -\frac{q_\varepsilon^2}{\pi} \frac{2\lambda + \sqrt{2\kappa \rho_w c_p^w \omega}}{(\lambda^2 + \kappa \rho_w c_p^w \omega + \lambda \sqrt{2\kappa \rho_w c_p^w \omega})^2}. \tag{25}$$

First of all, it should be noted that power spectra of SST fluctuations have been explored on several occasions previously via both observations and numerical simulations (e.g., [37–39,44–47,73–79]). The results of these studies show, in particular, that power laws with a certain scaling exponent ζ approximate observed SST spectra quite well, i.e., $S_T(\nu) \propto \nu^{-\zeta}$, where ν is a regular frequency. The value of ζ depends on a number of factors, such as time scales of processes, geographical region is a question, and the underlined surface type [79]. For example, in [79], the spectrum of global mean temperature variability was estimated using the gridded dataset of global historical surface temperature anomalies HadCRUT4. For the frequency range corresponding to intra-annual time scales, the scaling exponent was 0.80 ± 0.15 . Almost identical results were obtained in [78,80].

Figure 1 shows spectra of SSTA simulated by different models used in this study. It is important to point out that in the ocean–atmosphere system, the formation mechanisms of SST variability are highly complicated. Therefore, it would be naive to expect that the extremely simple models are able to reproduce the theoretical spectra of SST fluctuations in complete agreement with the observed spectra. However, there are regions of the

global ocean that are dynamically inactive in relative terms. Such a region is, for example, the north-eastern part of the Pacific Ocean. Here, vertical motions are negligible, and the average annual current speeds are less than 0.5 cm/s. For such regions, observed and simulated SST spectra are in good agreement with each other, and their shape in the high frequency range corresponds to the ν^{-2} pattern, while at low frequencies the spectra tend to a constant value. These results allow us to make the conclusion that in the dynamically inactive ocean regions, the SST variability is mainly produced by the local ocean–atmosphere interactions and can be described by linear stochastic models such as one-box and two-box considered above. Meanwhile, there are areas of the global ocean in which the observed SST spectra on the intra-annual time scale do not obey the ν^{-2} law and, therefore, cannot be simulated by linear one- and two-box stochastic models. Such areas include, for example, the subtropics of the North Atlantic, the north-western part of the Pacific Ocean, and the Southern Ocean. In these areas, the formation mechanisms of SSTA are mainly determined by ocean circulation rather than by local ocean–atmosphere interactions [73–75]. The diffusion model can, to some extent, serve as a suitable tool for simulating SSTA in such areas of the global ocean.

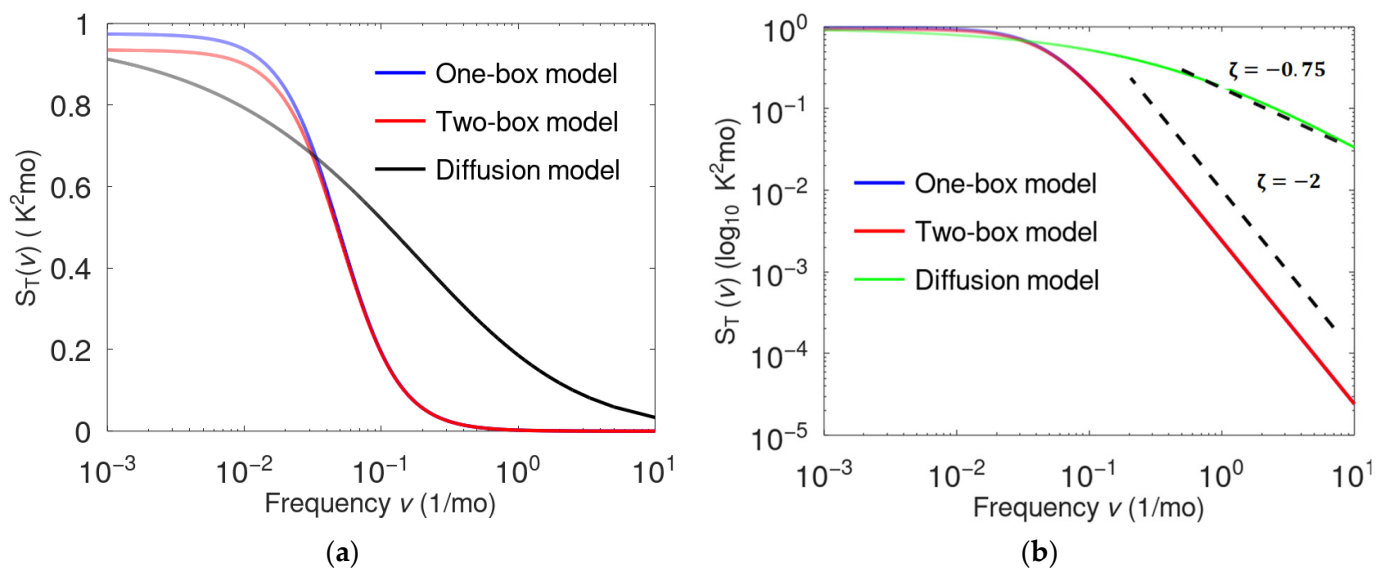


Figure 1. Power spectra of SSTA derived from one-box, two-box and diffusion models: (a) Semi-log plot; (b) log–log plot with dashed lines that show the characteristic ν^{-2} and $\nu^{-0.75}$ slopes.

For the concise comparative analysis of theoretical and observed power spectra of SSTA, we computed four PSD for different geographical regions. Figure 2 provides the power spectra of SSTA in two tropical regions of the Atlantic. The PSD of Tropical North Atlantic SSTA (TNA SSTA) is shown in Figure 2a, while the PSD of Tropical South Atlantic SSTA (TSA SSTA) is depicted in Figure 2b. The TNA SSTA are obtained from monthly mean SSTA averaged over the region ($5.5^\circ N$ – $23.5^\circ N$ and $15^\circ W$ – $57.5^\circ W$), and the TSA SSTA are derived from monthly mean SSTA averaged over the region south of the Equator ($Equator$ – $20^\circ S$ and $10^\circ E$ – $30^\circ W$). Time series of monthly mean SSTA obtained from the NOAA Physical Sciences Laboratory cover the period 1948–2023. On intra-annual time scales, the calculated PSD scaling exponents vary in the range of $-1.7 \leq \zeta \leq -1.5$. Note that the slope of the SST spectrum can be determined by applying a linear regression in the log–log coordinate system to a specific spectrum’s frequency range.

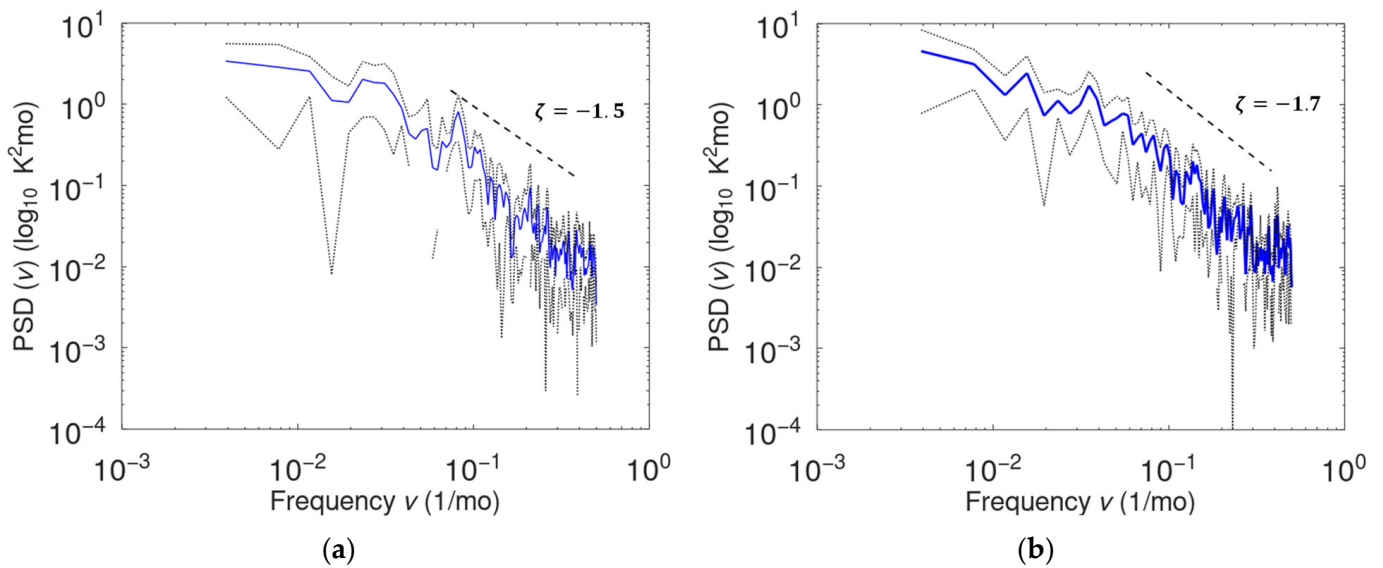


Figure 2. Observed power spectra of the tropical Atlantic SSTA: (a) the power spectral density of Tropical North Atlantic SSTA; (b) the power spectral density of Tropical South Atlantic SSTA. The Tropical North Atlantic SSTA are obtained from monthly mean SSTA averaged over the region (5.5° N–23.5° N and 15° W–57.5° W), while the Tropical South Atlantic SSTA are derived from monthly mean SSTA averaged over the region south of the Equator (Equator–20° S and 10° E–30° W). Time series of monthly mean SSTA cover the period 1948–2023 (<https://psl.noaa.gov/data/climateindices/list>, accessed on 22 September 2023). Dotted grey lines represent the 95% confidence interval. Dashed lines show spectral slopes.

Spectra of observed SST fluctuations calculated for two randomly chosen mid-latitude regions are shown in Figure 3 (we should note that partitioning the world’s ocean into regions based on the similarity of power spectra is a time-consuming problem that requires specific consideration). The left panel displays the PSD of mid-latitude North Atlantic SSTA, which are derived from monthly mean SSTA averaged over the region (35° N–45° N and 35° W–45° W), while the right panel presents the PSD of mid-latitude North Pacific SSTA that are monthly mean SSTA averaged over the region (35° N–45° N and 155° W–165° W). Time series of monthly mean SSTA obtained from the Met Office Hadley Centre cover the period 1945–2020. Estimated values of scaling exponents for PSD on the intra-annual time scales vary in the range between -1.2 and -0.9 . A rather powerful peak at a frequency $\nu \approx 0.083 \text{ mo}^{-1}$ is clearly visible in the mid-latitude spectra. The period associated with this cycle is the usual 12-month seasonal variability (seasonality).

Feedback parameter λ , as mentioned earlier, is the parameter with inherent uncertainty. To estimate the effect of this uncertainty on the power spectrum of SST, we can use the sensitivity function, which is defined as a partial derivative of PSD S_T with respect to λ , that is $\Psi_\lambda = \partial S_T / \partial \lambda$. Using Ψ_λ , we can, as a first approximation, quantify the influence of uncertainty in the parameter λ on the corresponding uncertainty in the PSD, namely $\Delta S_T \approx \Delta \lambda \cdot \Psi_\lambda$. Thus, sensitivity function Ψ_λ characterizes the response of the power spectrum to changes in the feedback parameter.

Figure 4 shows the sensitivity functions of PSD with respect to the parameter λ , calculated in the frequency domain for the one-box, two-box, and diffusion models. From this figure, it is clear that the absolute values of sensitivity functions increase with decreasing oscillation period, and this increase is nonlinear. On intra-annual time scales, the dependence of PSD on the parameter λ obtained for the one-box and two-box models is insignificant. For example, for SST fluctuations with an annual period, the absolute values of $\Psi_\lambda^{(1)}$ and $\Psi_\lambda^{(2)}$ are practically identical and equal approximately to $1.2 \cdot 10^{-2} \text{ K}^2\text{mo} / (\text{Wm}^{-2}\text{K}^{-1})$, while for fluctuations with a six-month period, the absolute values of $\Psi_\lambda^{(1)}$ and $\Psi_\lambda^{(2)}$ are

about $10^{-3} \text{ K}^2\text{mo}/(\text{Wm}^{-2}\text{K}^{-1})$. Meanwhile, on inter-annual and intra-annual time scales, the diffusion model PSD demonstrates significantly greater sensitivity to changes in the parameter λ . For fluctuations with one-year and six-month periods, the absolute values of sensitivity function $\Psi_\lambda^{(3)}$ are $7.2 \cdot 10^{-2}$ and $5 \cdot 10^{-2} \text{ K}^2\text{mo}/(\text{Wm}^{-2}\text{K}^{-1})$, respectively. It should be noted that sensitivity functions are usually used when the variations in the affecting parameter are small enough, ideally infinitesimal. If the parameter variations are quite large, the direct modeling is applied to estimate the effect of these variations on the model output. Figure 5 presents PSD computed for the base value of the feedback parameter $\lambda_0 = 35 \text{ Wm}^{-2}\text{K}^{-1}$ and the perturbed parameter $\lambda = \lambda_0 \pm \Delta$, where Δ is 10% change in base value of the feedback parameter. Calculations were performed using a one-box model (left panel) and a diffusion model (right panel). Figure 5 shows that on intra-annual timescales, uncertainty in the parameter λ has little effect on the power spectrum. Variations in the parameter λ more or less noticeably affect the power spectrum on inter-annual and longer time scales. The power spectrum calculated using the diffusion model is more sensitive to changes in the feedback parameter than the power spectrum obtained using the one-box or two-box model. In general, the accuracy of determining the feedback parameter is not critical when modeling SSTA on intra-annual time scales.

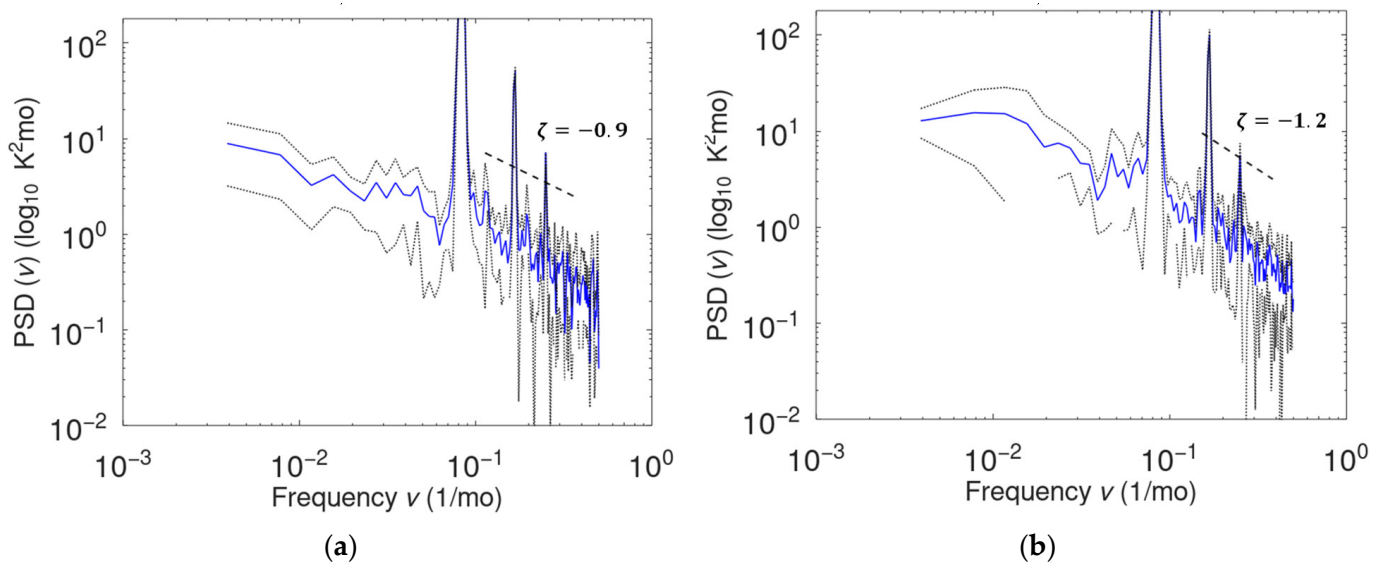


Figure 3. Observed power spectra of mid-latitude SSTA: (a) the power spectral density of mid-latitude North Atlantic SSTA; (b) the power spectral density of mid-latitude North Pacific SSTA. The mid-latitude North Atlantic SST anomalies are obtained from monthly mean SSTA averaged over the region (35° N – 45° N and 35° W – 45° W), while the mid-latitude North Pacific SSTA are derived from monthly mean SSTA averaged in the region (35° N – 45° N and 155° W – 165° W). Time series of monthly mean SSTA cover the period 1945–2020 (<https://www.metoffice.gov.uk/hadobs/en4/>, accessed on 22 September 2023). Dotted grey lines represent the 95% confidence interval. Dashed lines show the spectral slopes.

When analyzing obtained results, it is necessary not to demand more from the local statistical theory than it is capable of providing. Indeed, it is naive to hope to describe the SST variability over the entire frequency range with any given simple “unified” model. This is hardly possible, if only because the object of study itself, the ocean mixed layer, changes seasonally. The physics of processes at different time scales also do not remain the same. Therefore, it is more fruitful not to emphasize the differences, which should be obvious anyway, but, on the contrary, to pay attention to the similarity of the empirical spectra to what is prescribed by simple local statistical theory. This is precisely what was done in the first papers published on this topic by Hasselmann [49] and Frankignoul and Hasselmann [37]. The results obtained confirm that the application of local statistical theory

is very useful for describing and interpreting the variability of the ocean’s thermal state. It should also be noted that the results of our study do not contradict the results of previously conducted research.

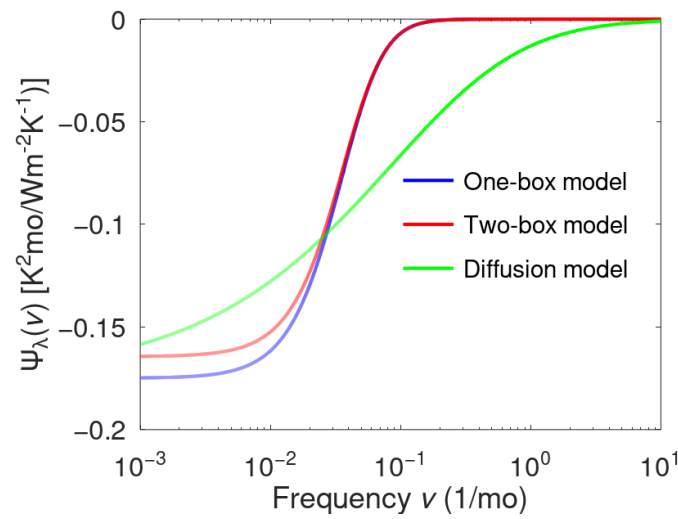


Figure 4. Sensitivity functions of power spectral density with respect to parameter λ for one-box, two-box, and diffusion models.

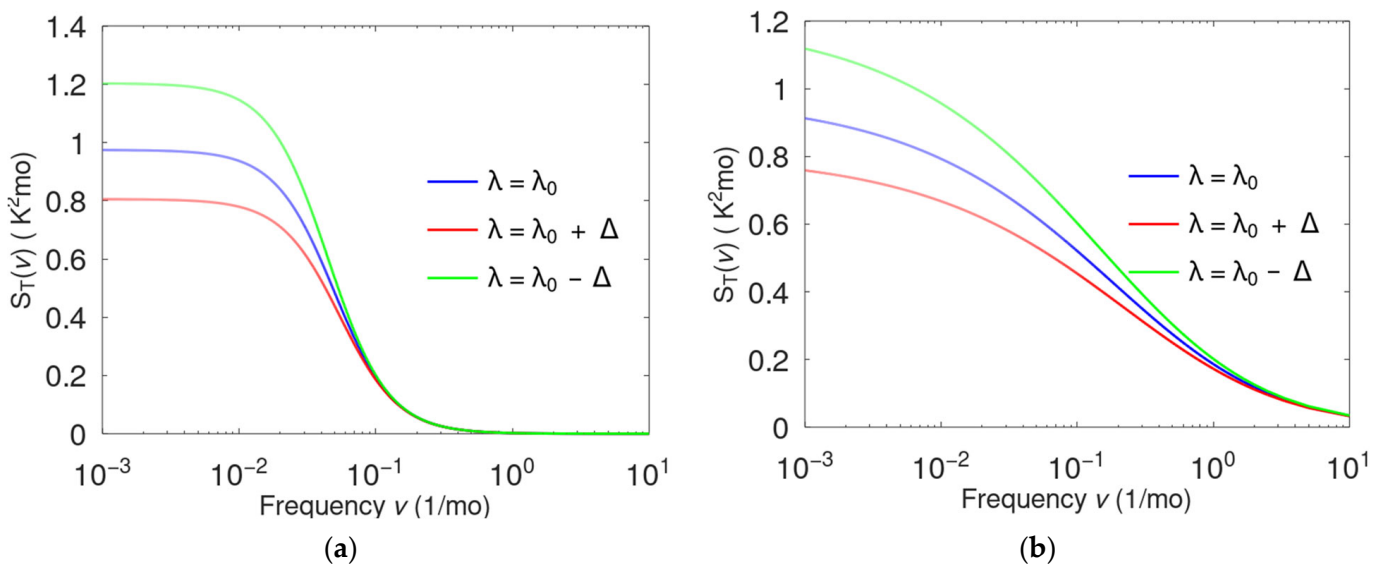


Figure 5. Power spectral density calculated for the base value of the feedback parameter $\lambda_0 = 35 \text{ Wm}^{-2}\text{K}^{-1}$ and the perturbed parameter $\lambda = \lambda_0 \pm \Delta$, where $\Delta = 0.1 \times \lambda_0$ (i.e., Δ is 10% change in base value of the feedback parameter): (a) one-box model; (b) diffusion model.

Thus, examined simple linear stochastic models describing local ocean–atmosphere interactions are able to provide a physically plausible, at least qualitative, simulation of power spectra of SST fluctuations on intra-annual time scales. However, the empirical correlation time of SST fluctuations may exceed the estimate obtained using conceptual stochastic models considered above [46,47,49,62,77] (Figure 6 shows this effect). This is largely because simple models do not account for non-local processes of ocean–atmosphere interactions and, therefore, the non-locality of atmospheric temperature response to SSTA.

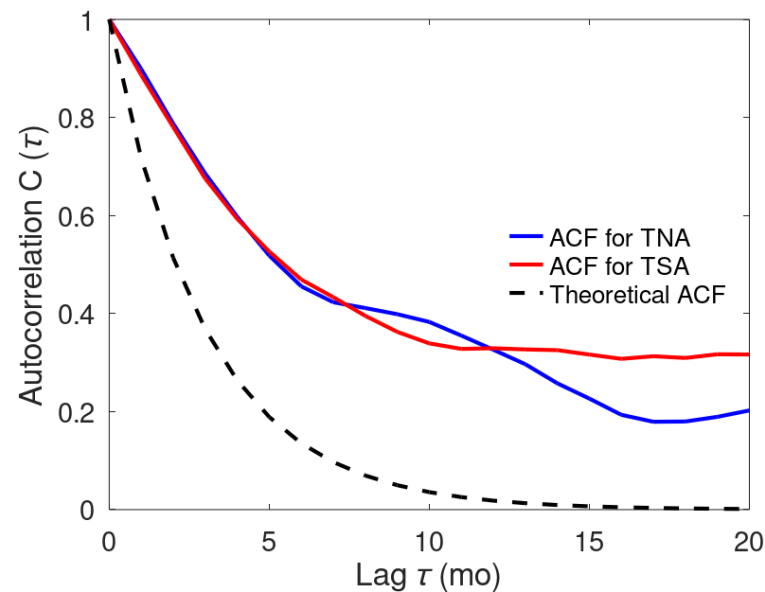


Figure 6. Theoretical autocorrelation function (ACF) of the random process described by the one-box model (black dashed line), and ACF for Tropical North Atlantic SSTA (blue) and ACF for Tropical South Atlantic SSTA (red). SSTA from 1948 to 2023 were derived from NOAA SST data (<https://psl.noaa.gov/>).

Nevertheless, the low-order stochastic models presented in this paper, describing local ocean–atmosphere interactions, as well as the technique for estimating the sensitivity of SST fluctuation power spectra to variations in the feedback parameter, can serve as a theoretical tool for exploring the SST variability in different parts of the world’s ocean on intra-annual timescales, taking into account the uncertainties in the feedback parameter. The value of these models in practice is determined by the fact that all quantities describing the random process of SST anomaly formation can be estimated directly from the heat balance equation of the mixed ocean layer.

4. Conclusions

Despite significant advances in long-term weather forecasting achieved in recent years, the accuracy of these forecasts remains quite low. As shown in a number of studies, the formation of weather and climate in the middle and high latitudes of the Eurasian continent is significantly affected by SSTA in the tropical North Atlantic. To better understand these effects, as well as to develop new methods for long-term weather forecasting based on machine learning, further study of SST variability in different parts of the world’s oceans is required. In this context, conceptual climate models are effective research tools that allow one to estimate the influence of various physical factors on the SSTA. In this paper, we considered simple models, which can be used to study the influence of local effects due to ocean–atmosphere interactions on SST variability. To explore non-local effects, highly complex coupled ocean–atmosphere general circulation models are a valuable tool, requiring vast intellectual and computational resources for the formulation and implementation of numerical experiments. Nevertheless, sometimes, to examine the essential features of non-local effects, conceptual models can be used that, in a simplified manner, describe the atmosphere–ocean interactions while accounting for horizontal large-scale heat exchange. An example of how non-local effects can be included in stochastic models was discussed in the paper of Lemke [57], in which the author applied a non-local stochastic model to explore surface temperature variability over time scales ranging from 10 to 10^4 years. However, the study of non-local effects of atmosphere–ocean interactions is beyond the scope of this paper and will be addressed separately.

Funding: This research was funded by RSF, grant number 23-47-10003.

Institutional Review Board Statement: Not applicable.

Informed Consent Statement: Not applicable.

Data Availability Statement: All data used in this study are available upon request.

Acknowledgments: The author would like to thank Paul Sukhonos for technical support in preparation time series of monthly mean SSTA in the mid-latitude North Atlantic and mid-latitude North Pacific.

Conflicts of Interest: The author declares no conflicts of interest.

Appendix A

Long-range weather forecasting commonly comes down to predicting anomalies of meteorological variables and weather phenomena, primarily surface air temperature and precipitation anomalies, averaged over some sufficiently large region, having an area in the order of several thousand square kilometers and a lead time of a few months. In such cases, synoptic-scale atmospheric processes can be looked at through the lens of statistical averages. In other words, relatively rapid fluctuations in atmospheric processes, involving effects of continuous interaction with the ocean, can be considered as noise that does not significantly affect the average state of the climate system (the first moment), which is mainly determined by slow and stable processes, but affects only the variability of the climate system (second moment). To develop new methods of long-range weather forecasting, it is highly desirable to have a priori information on how sensitive temperature anomalies in a particular region are to variations in weather and climate conditions, including sea surface temperature variations, in remote areas of the planet. Putting it differently, the study of asynchronous statistical relationships between weather anomalies in remote regions and subsequent weather anomalies in the region under consideration is extremely important for understanding the processes occurring in the climate system and, consequently, for developing reliable methods for long-term forecasting. Additionally, it should be noted that the local state of the atmosphere is very sensitive to unpredictable “meteorological weather noise”. Nevertheless, to date, global coupled ocean–atmosphere models remain key tools for studying large-scale interaction between ocean and atmosphere and estimating the ocean’s role in the formation of weather and climate. Meanwhile, to study asynchronous relationships between weather anomalies in different geographical regions, one can also apply the mathematical concept of adjoint equations, whereas the effects of weather noise on large-scale characteristics of the atmosphere and ocean can be explored within the framework of quasi-local theory using simple stochastic models of the climate system, in which the weather noise is represented as a random process with specified properties.

A historical digression into the theory of adjoint equations and their applications for sensitivity analysis of linear and nonlinear systems can be found in [81]. The fundamentals of the theory of sensitivity for linear and nonlinear systems based on the adjoint method are described in [82–84]. To illustrate the main idea of the adjoint-based approach, let us consider a simple evolutionary differential equation:

$$\begin{aligned} \frac{\partial \phi}{\partial t} + \mathcal{L}\phi &= f \text{ in } (0, t_f] \times \mathcal{D}, \\ \phi &= \phi_0 \text{ at } t = 0, \end{aligned} \tag{A1}$$

where $\phi(t, x)$ is the state variable with $\text{dom}\phi = \mathcal{D}$; $t \in [0, t_f]$ is time; \mathcal{L} is linear operator; $f(t, x)$ is some function.

Defining the adjoint operator via the Lagrange’s identity as $(\mathcal{L}\phi, \phi^*) = (\phi, \mathcal{L}^*\phi^*)$, where (\cdot, \cdot) is a dot product, we can write the adjoint equation as

$$\begin{aligned} -\frac{\partial \phi^*}{\partial t} + \mathcal{L}^*\phi^* &= f^* \text{ in } (0, T] \times \mathcal{D}, \\ \phi^* &= \phi_T^* \text{ at } t = t_f. \end{aligned} \tag{A2}$$

Here, f^* and $\phi_{t_f}^*$ are some yet undefined functions, the specific form of which is determined based on the physical meaning of the problem under consideration.

Multiplying (1) by scalar ϕ , and (2) by scalar ϕ^* , subtracting the first equation from the second one and then integrating the obtained result over time from initial time, 0, to some final time, t_f , we get the following relation:

$$(\phi, \phi^*)_{t_f} - (\phi, \phi^*)_0 = \int_0^{t_f} [(f, \phi^*) - (\phi, f^*)] dt. \quad (\text{A3})$$

Note that $\phi_{t_f} = \phi(t_f, x)$ and $\phi_0^* = \phi^*(0, x)$. Now we can choose functions f^* and ϕ_T^* . For example, we can take $\phi_{t_f}^* = 0$ and $f^* = 1$ in selected subdomain $\mathcal{D}_\phi \subset \mathcal{D}$, then

$$\bar{\phi} = \frac{1}{\text{mes}(\mathcal{D}_\phi)} \left[(\phi_0, \phi_0^*) - \int_0^{t_f} (f, \phi^*) dt \right]. \quad (\text{A4})$$

Here, the quantity $\bar{\phi}$ is the value of function ϕ averaged over the subdomain \mathcal{D}_ϕ and time interval $0 \leq t \leq t_f$; ϕ^* is the influence function; and $\text{mes}(\mathcal{D}_\phi)$ is the measure of \mathcal{D}_ϕ (length, area, volume). Note that if \mathcal{L} is a nonlinear operator, then the problem becomes more complicated [83–85]; however, the basic idea of the method remains the same.

The use of adjoint equations for the analysis and long-term forecasting of temperature anomalies was demonstrated, for example, in [85,86]. As shown in these papers, isolines of adjoint functions (influence functions) quantify the degree of influence of heat exchange processes between the atmosphere and ocean on the formation of temperature anomalies in remote areas. The areas with the highest values of the adjoint functions were called energy-active zones of the ocean, since in these areas the atmosphere-ocean heat exchange reaches its maximum.

References

1. IPCC. *Climate Change 2022: Impacts, Adaptation, and Vulnerability*; Contribution of Working Group II to the Sixth Assessment Report of the Intergovernmental Panel on Climate Change; Pörtner, H.-O., Roberts, D.C., Tignor, M., Poloczanska, E.S., Mintenbeck, K., Alegria, A., Craig, M., Langsdorf, S., Löschke, S., Möller, V., et al., Eds.; Cambridge University Press: Cambridge, UK; New York, NY, USA, 2022; 3056p. [\[CrossRef\]](#)
2. Staniforth, A.; Mailhot, J. An operational model for regional weather prediction. *Comput. Math. Appl.* **1988**, *16*, 1–22. [\[CrossRef\]](#)
3. Kalnay, E. *Atmospheric Modeling, Data Assimilation and Predictability*; Cambridge University Press: Cambridge, UK, 2002. [\[CrossRef\]](#)
4. Orrell, D.; Smith, L.; Barkmeijer, J.; Palmer, T. Model error in weather forecasting. *Nonlinear Process. Geophys.* **2001**, *8*, 357–371. [\[CrossRef\]](#)
5. Privé, N.; Errico, R.; Tai, K.-S. The influence of observation errors on analysis error and forecast skill investigated with an observing system simulation experiment. *J. Geophys. Res.* **2013**, *118*, 5332–5346. [\[CrossRef\]](#)
6. Pu, Z.-X.; Kanay, E.; Sela, J.; Szunyogh, I. Sensitivity of forecast error to initial conditions with a quasi-inverse linear method. *Mon. Weather Rev.* **1997**, *125*, 2479–2503. [\[CrossRef\]](#)
7. Thompson, P.D. Uncertainty of initial state as a factor in the predictability of large-scale atmospheric flow patterns. *Tellus* **1957**, *9*, 275–295. [\[CrossRef\]](#)
8. Lorenz, E. A study of the predictability of a 28-variable atmospheric model. *Tellus* **1965**, *17*, 321–333. [\[CrossRef\]](#)
9. Lorenz, E. The predictability of a flow which possesses many scales of motion. *Tellus* **1969**, *21*, 289–307. [\[CrossRef\]](#)
10. Lorenz, E.N. Atmospheric predictability experiments with a large numerical model. *Tellus* **1982**, *34*, 505–513. [\[CrossRef\]](#)
11. Zhang, F.; Sun, Y.Q.; Magnusson, L.; Buizza, R.; Chen, J.-H.; Emanuel, K. What is the predictability limit of midlatitude weather? *J. Atmos. Sci.* **2019**, *74*, 1077–1091. [\[CrossRef\]](#)
12. Monin, A.S. *Introduction of the Theory of Climate*; Hydrometeoizdat: Leningrad, Russia, 1982; 246p.
13. Arguez, A.; Vose, R. The definition of the standard WMO climate normal. *Bull. Am. Meteorol. Soc.* **2011**, *92*, 699–704. [\[CrossRef\]](#)
14. Coiffier, J. *Fundamentals of Numerical Weather Prediction*; Cambridge University Press: Cambridge, UK, 2012; 368p.
15. Bauer, P.; Thorpe, A.; Brunet, G. The quiet revolution on numerical weather prediction. *Nature* **2015**, *525*, 47–55. [\[CrossRef\]](#)
16. Palmer, T.N. *Predicting Uncertainty in Forecasts of Weather and Climate*; ECMWF Technical Memorandum No. 294; ECMWF; Shinfield Park: Reading, UK, 1999.
17. Alexandrov, V. Using Better Climate Prediction in the Implementation of National Action Programmes—(Eastern Europe). In *Climate and Land Degradation*; Sivakumar, M.V.K., Ndiang’yi, N., Eds.; Springer: Berlin/Heidelberg, Germany, 2007; pp. 537–551. [\[CrossRef\]](#)

18. Garcia-Soto, C.; Cheng, L.; Caesar, L.; Schmidtko, S.; Jewett, E.B.; Cheripka, A.; Rigor, I.; Caballero, A.; Chiba, S.; Báez, J.C.; et al. An Overview of Ocean Climate Change Indicators: Sea Surface Temperature, Ocean Heat Content, Ocean pH, Dissolved Oxygen Concentration, Arctic Sea Ice Extent, Thickness and Volume, Sea Level and Strength of the AMOC (Atlantic Meridional Overturning Circulation). *Front. Mar. Sci.* **2021**, *8*, 642327. [[CrossRef](#)]
19. Köhl, A.; Vlasenko, A. Seasonal prediction of northern European winter air temperatures from SST anomalies based on sensitivity estimates. *Geophys. Res. Lett.* **2019**, *46*, 6109–6117. [[CrossRef](#)]
20. Lorenz, E.N. Deterministic nonperiodic flow. *J. Atmos. Sci.* **1963**, *20*, 130–141. [[CrossRef](#)]
21. Boukabara, S.-A.; Krasnoposky, V.; Penny, S.G.; Stewart, J.Q.; McGovern, A.; Hall, D.; Hoeve, J.E.T.; Hickey, J.; Huang, H.-L.A.; Williams, J.K.; et al. Outlook for exploiting artificial intelligence in the earth and environmental sciences. *Bull. Am. Meteorol. Soc.* **2021**, *102*, E1016–E1032. [[CrossRef](#)]
22. Bochenek, B.; Ustrnul, Z. Machine learning in weather prediction and climate analyses—Applications and perspectives. *Atmosphere* **2022**, *13*, 180. [[CrossRef](#)]
23. Dewitte, S.; Cornelis, J.P.; Müller, R.; Munteanu, A. Artificial intelligence revolutionises weather forecast, climate monitoring and decadal prediction. *Remote Sens.* **2021**, *13*, 3209. [[CrossRef](#)]
24. Lam, R.; Sanches-Gonzales, A.; Willson, M.; Wirnsberger, P.; Fortunato, M.; Alet, F.; Ravuri, S.; Ewalds, T.; Eaton-Rosen, Z.; Hu, W.; et al. Learning skillful medium-range global weather forecasting. *Science* **2023**, *382*, 1416–1421. [[CrossRef](#)]
25. Li, J.; Wang, Z.; Wu, X.; Xu, C.; Guo, S.; Chen, X.; Zhang, Z. Robust meteorological drought prediction using antecedent SST fluctuations and machine learning. *Water Resour. Res.* **2021**, *57*, e2020WR029413. [[CrossRef](#)]
26. Hatsuzuka, D.; Sato, T. Impact of SST on present and future extreme precipitation in Hokkaido investigated considering weather. *JGR Atmos.* **2022**, *127*, e2021JD036120. [[CrossRef](#)]
27. Melhauser, C.; Li, W.; Zhu, Y.; Zhou, X.; Peña, M.; Hou, D. Exploring the Impact of SST on the Extended Range NCEP Global Ensemble Forecast System. In Proceedings of the 41st NOAA Annual Climate Diagnostics and Prediction Workshop, Orono, ME, USA, 3–6 October 2016.
28. Climate Indicators: Sea Surface Temperature. Available online: <https://climate.copernicus.eu/climate-indicators/sea-surface-temperature> (accessed on 11 June 2023).
29. Alekseev, G.V.; Glok, N.I.; Vyazilova, A.E.; Kharlanenkova, N.E.; Kulakov, M.Y. Influence of SST in Low Latitudes on the Arctic Warming and Sea Ice. *J. Mar. Sci. Eng.* **2021**, *9*, 1145. [[CrossRef](#)]
30. Alekseev, G.; Kuzmina, S.; Bobylev, L.; Urazgildeeva, A.; Gnatiuk, N. Impact of atmospheric heat and moisture transport on the Arctic warming. *Int. J. Climatol.* **2019**, *39*, 3582–3592. [[CrossRef](#)]
31. Årthun, M.; Eldevik, T. On anomalous ocean heat transport toward the Arctic and associated climate predictability. *J. Clim.* **2016**, *29*, 689–704. [[CrossRef](#)]
32. Arthun, M.; Eldevik, T.; Smedsrud, L.H.; Skagseth, Ø.; Ingvaldsen, R.B. Quantifying the influence of Atlantic heat on Barents sea ice variability and retreat. *J. Clim.* **2012**, *25*, 4736–4743. [[CrossRef](#)]
33. Thomson, S.; Vallis, G. Atmospheric response to SST anomalies. Part I: Background-state dependence, teleconnections, and local effects in winter. *J. Atmos. Sci.* **2018**, *75*, 4107–4124. [[CrossRef](#)]
34. Armour, K.C.; Siler, N.; Donohoe, A.; Roe, G.H. Meridional atmospheric heat transport constrained by energetics and mediated by large-scale diffusion. *J. Clim.* **2019**, *32*, 3655–3680. [[CrossRef](#)]
35. Soldatenko, S. Estimated impacts of climate change on eddy meridional moisture transport in the atmosphere. *Appl. Sci.* **2019**, *9*, 4992. [[CrossRef](#)]
36. Bjerknes, J. Atlantic air-sea interaction. *Adv. Geophys.* **1964**, *10*, 1–82.
37. Frankignoul, C.; Hasselmann, K. Stochastic climate models. Part II. Application to seasurface temperature anomalies and thermocline variability. *Tellus* **1977**, *29*, 284–305.
38. Battisti, D.S.; Bhatt, U.S.; Alexander, M.A. A modeling study of the interannual variability in the wintertime North Atlantic Ocean. *J. Clim.* **1995**, *8*, 3067–3083. [[CrossRef](#)]
39. Delworth, T.L. North Atlantic interannual variability in a coupled ocean-atmosphere model. *J. Clim.* **1996**, *9*, 2356–2375. [[CrossRef](#)]
40. Zorita, E.; Kharin, V.; von Storch, H. *The Atmospheric Circulation and Sea Surface Temperature in the North Atlantic Area In winter: Their Interaction and Relevance for Iberian Precipitation*; Rep. 54; Max-Planck Institut fuer Meteorologie: Hamburg, Germany, 1999; 22p.
41. Cayan, D.R. Latent and sensible heat flux anomalies over the northern oceans: Driving the sea surface temperature. *J. Phys. Oceanogr.* **1992**, *22*, 859–881. [[CrossRef](#)]
42. Moisan, J.R.; Niiler, P.P. The seasonal heat budget of the north Pacific: Net heat flux and heat storage rates (1950–1990). *J. Phys. Oceanogr.* **1998**, *28*, 401–421. [[CrossRef](#)]
43. Vijith, V.; Vinayachandran, P.N.; Webber, B.G.M.; Matthews, A.J.; George, J.V.; Kannaujia, V.K.; Lotliker, A.A.; Amol, P. Closing the sea surface mixed layer temperature budget from in situ observations alone: Operation Advection during BoBBLE. *Sci. Rep.* **2020**, *10*, 7062. [[CrossRef](#)]
44. Alexander, M.A.; Penland, C. Variability in a mixed layer ocean model driven by stochastic atmospheric forcing. *J. Clim.* **1996**, *9*, 2424–2442. [[CrossRef](#)]
45. Sura, P.; Newman, M.; Alexander, M.A. Daily to decadal sea surface temperature variability driven by state-dependent stochastic heat fluxes. *J. Phys. Oceanogr.* **2006**, *36*, 1940–1958. [[CrossRef](#)]

46. Demchenko, P.F.; Kislov, A.V. *Stochastic Dynamics of Natural Objects. Brownian Motion and Geophysical Applications*; GEOS: Moscow, Russia, 2010; 190p.
47. Liu, G.; Kwon, Y.; Frankignoul, C.; Lu, J. Understanding the drivers of Atlantic multidecadal variability using a stochastic model hierarchy. *J. Clim.* **2023**, *36*, 1043–1058. [[CrossRef](#)]
48. Pond, S.; Fissel, D.B.; Paulson, C.A. A note on bulk aerodynamic coefficients for sensible and latent heat and moisture fluxes. *Bound.-Layer Meteorol.* **1974**, *6*, 333–339. [[CrossRef](#)]
49. Hasselmann, K. Stochastic climate models, Part I: Theory. *Tellus* **1976**, *28*, 473–485.
50. Shi, H.; Jin, F.-F.; Wills, R.C.J.; Amaya, D.J.; Black, B.A.; Rykaczewski, R.R.; Bograd, S.J.; García-Reyes, M.; Sydeman, W.J. Global decline in ocean memory over the 21st century. *Sci. Adv.* **2022**, *8*, eabm3468. [[CrossRef](#)]
51. Piterbarg, L.I. *Dynamics and Forecast of Large-Scale Ocean Surface Temperature Anomalies*; Hydrometeoizdat: Leningrad, Russia, 1986; 200p.
52. Archer, C.I.; Jacobson, M.Z. Evaluation of global wind power. *J. Geophys. Res.* **2005**, *110*, D12110. [[CrossRef](#)]
53. Oliver, J.E. Bowen ratio. In *Climatology. Encyclopedia of Earth Science*; Springer: Boston, MA, USA, 1987. [[CrossRef](#)]
54. Munk, W.; Wunsch, C. Abyssal recipes II: Energetics of tidal and wind mixing. *Deep Sea Res. Part I Oceanogr. Res. Pap.* **1998**, *45*, 1977–2010. [[CrossRef](#)]
55. Feng, X.; Hainesaand, K.; de Boisseson, E. Coupling of surface air and sea surface temperatures in the CERA-20C reanalysis. *Q. J. R. Meteorol. Soc.* **2018**, *144*, 195–207. [[CrossRef](#)]
56. Kallberg, P.; Berrisford, P.; Hoskins, B.J.; Simmons, A.; Uppala, S.; Lamy-Thépaut, S.; Hine, R. *ERA-40 Atlas*; ERA-40 Project Report Series 19; ECMWF: Reading, UK, 2005; 199p.
57. Lemke, P. Stochastic climate models, Part 3: Application to zonally averaged energy models. *Tellus* **1977**, *29*, 385–392. [[CrossRef](#)]
58. Müller, P. Hasselmann's stochastic climate model viewed from a statistical mechanics perspective. In *Stochastic Climate Models. Progress in Probability*; Imkeller, P., von Storch, J.S., Eds.; Birkhäuser: Basel, Switzerland, 2001; Volume 49, pp. 285–295.
59. Franzke, C.L.E.; Blender, R.; O'Kane, T.J.O.; Lembo, V. Stochastic methods and complexity in climate research and modeling. *Front. Phys.* **2022**, *10*, 931596. [[CrossRef](#)]
60. Soldatenko, S.; Colman, R. Climate variability from annual to multi-decadal time scales in a two-layer stochastic energy balance model: Analytic solutions. *Tellus* **2019**, *71*, 1554421. [[CrossRef](#)]
61. Colman, R.; Soldatenko, S. Understanding the links between climate feedbacks, variability and change using a two-layer energy balance model. *Clim. Dyn.* **2020**, *54*, 3441–3459. [[CrossRef](#)]
62. Frankignoul, C. Stochastic forcing models of climate variability. *Dyn. Atmos. Oceans* **1979**, *3*, 465–479. [[CrossRef](#)]
63. Klyackin, V.I. *Lectures on Dynamics of Stochastic Systems*; Elsevier: Amsterdam, The Netherlands, 2010; 410p.
64. Gregory, J.M. Vertical heat transport in the ocean and their effect on time-dependent climate change. *Clim. Dyn.* **2000**, *16*, 501–515. [[CrossRef](#)]
65. Held, I.M.; Winton, M.; Takahashi, K.; Delworth, T.; Zeng, F.; Vallis, G.K. Probing the fast and slow components of global warming by returning abruptly to preindustrial forcing. *J. Clim.* **2010**, *23*, 2418–2427. [[CrossRef](#)]
66. Geoffroy, O.; Saint-Martin, D.; Olivie, D.J.L.; Voldoire, A.; Bellon, G.; Tytéca, S. Transient climate response in a two-layer energy-balance model. Part I: Analytical solution and parameter calibration using representation of the efficacy of deep-ocean heat uptake and validation for CMIP5 AOGCMs. *J. Clim.* **2013**, *26*, 1841–1857. [[CrossRef](#)]
67. Lebedeff, S.A. Analytic solution of the box diffusion model for a global ocean. *J. Geophys. Res.* **1988**, *93*, 14243–14255. [[CrossRef](#)]
68. Hodnett, P.F.; McNamara, R. On the spatial variation of the vertical thermal diffusion coefficient in a simple ocean model. *Math. Proc. R. Ir. Acad.* **2003**, *103A*, 217–230. [[CrossRef](#)]
69. Yaglom, A.M. *Correlation Theory of Stationary and Related Random Functions, Volume I: Basic Results*; Springer: New York, NY, USA, 1987; 526p.
70. Gardiner, C. *Stochastic Methods: A Handbook for the Natural and Social Sciences*, 4th ed.; Springer: Berlin/Heidelberg, Germany, 2009; 447p.
71. Lathi, B.P. *Signal Processing and Linear Systems*, 2nd ed.; Oxford University Press: New York, NY, USA, 2009; 864p.
72. Leith, C.E. The standard error of time-average estimates of climatic means. *J. Appl. Meteorol. Climatol.* **1973**, *12*, 1066–1069. [[CrossRef](#)]
73. Demchenko, P.F. A simple statistical model of ocean surface temperature anomalies with allowance for concomitant changes in air temperature. *Atmos. Ocean. Phys.* **1987**, *23*, 399–404.
74. Manabe, S.; Stouffer, R. Low-frequency variability of surface air temperature in a 1000-year integration of a coupled atmosphere-ocean-land surface model. *J. Clim.* **1996**, *9*, 376–393. [[CrossRef](#)]
75. Hall, A.; Manabe, S. Can local linear stochastic theory explain sea surface temperature and salinity variability? *Clim. Dyn.* **1997**, *13*, 167–180. [[CrossRef](#)]
76. Pelletier, J.D. The power spectral density of atmospheric temperature from time scales of 10^{-2} to 10^6 yr. *Earth Planet. Sci. Lett.* **1998**, *158*, 157–164. [[CrossRef](#)]
77. Dommenges, D.; Latif, M. Analysis of observed and simulated SST spectra in the midlatitudes. *Clim. Dyn.* **2002**, *19*, 277–288. [[CrossRef](#)]
78. Fredriksen, H.; Rypdal, K. Spectral characteristics of instrumental and climate model surface temperatures. *J. Clim.* **2016**, *29*, 1253–1268. [[CrossRef](#)]

79. Zhu, F.; Emile-Geay, J.; McKay, N.P.; Hakim, G.J.; Khider, D.; Ault, T.R.; Steig, E.J.; Dee, S.; Kirchner, J.W. Climate models can correctly simulate the continuum of global-average temperature variability. *Proc. Natl. Acad. Sci. USA* **2019**, *116*, 8728–8733. [[CrossRef](#)] [[PubMed](#)]
80. Rypdal, M.; Rypdal, K. Long-memory effects in linear response models of Earth's temperature and implications for future global warming. *J. Clim.* **2014**, *27*, 5240–5258. [[CrossRef](#)]
81. Cacuci, D.G.; Schlesinger, M.E. On the application of the adjoint method of sensitivity analysis to problems in the atmospheric sciences. *Atmósfera* **1994**, *7*, 47–59.
82. Cacuci, D.G. *Sensitivity and Uncertainty Analysis: Theory*; Chapman & Hall/CRC: Boca Raton, FL, USA, 2003.
83. Cacuci, D.G.; Ionescu-Bujor, M.; Navon, M.I. *Sensitivity and Uncertainty Analysis: Applications to Large Scale Systems*; Chapman & Hall/CRC: Boca Raton, FL, USA, 2005.
84. Marhuck, G.I. *Adjoint Equations and Analysis of Complex System*; Kluwer Academic Publishers: Dordrecht, The Netherlands, 1995.
85. Marhuck, G.I.; Skiba, Y.N. Role of adjoint equations in estimating monthly mean air surface temperature anomalies. *Atmósfera* **1992**, *55*, 119–133.
86. Zaurbekov, N.S. Numerical analysis and forecast of anomalies of atmospheric processes using adjoint functions. *J. Math. Mech. Comput. Sci.* **2011**, *69*, 97–101.

Disclaimer/Publisher's Note: The statements, opinions and data contained in all publications are solely those of the individual author(s) and contributor(s) and not of MDPI and/or the editor(s). MDPI and/or the editor(s) disclaim responsibility for any injury to people or property resulting from any ideas, methods, instructions or products referred to in the content.